MAGMATIC AND POST-MAGMATIC SIGNATURES OF CHROMIAN SPINELS IN PODIFORM CHROMITITES FROM THE CHESHMEH-BID CHROMITITE DEPOSIT, KHAJEH-JAMALI OPHIOLITIC MASSIFS, IRAN

Alireza Eslami*, Majid Ghaderi*,✉, William L. Griffin, Sarah Gain**, Giovanni Grieco*** and José M. González-Jiménez°**

* *Department of Economic Geology, Tarbiat Modares University, Tehran, Iran.*
** *ARC Centre of Excellence for Core to Crust Fluid Systems (CCFS) and GEMOC, Department of Earth and Planetary Sciences, Macquarie University, Sydney, Australia.*
*** *Dipartimento di Scienze della Terra, Università degli Studi di Milano, Italy.*
° *Department of Geology and Andean Geothermal Center of Excellence (CEGA), Universidad de Chile, Santiago de Chile, Chile.*
✉ *Corresponding author, e-mail: mghaderi@modares.ac.ir*

Keywords: *Trace and minor elements, chromitite, Cheshmeh-Bid ore deposit, Late Cretaceous, Khajeh-Jamali ophiolitic massifs. Iran.*

ABSTRACT

Podiform bodies of high-Cr chromitite in the Cheshmeh-Bid chromitite deposit are located at the mantle-lower crust transition zone (MTZ) of the Late Cretaceous Khajeh-Jamali ophiolitic massifs, Iran. The unaltered core of chromian spinels has retained their magmatic composition but post magmatic subsolidus re-equilibration changed significantly minor and trace elements (Ga, Ti, Ni, Zn, Co, Mn, V and Sc) composition. Minor disseminated chromites also occur and show lower chromite/silicate ratios than massive chromitites and were much more affected by the subsolidus mobility of minor and trace elements. Using the composition of the unaltered chromites preserved in the cores we have estimated the Al content and Fe/Mg ratios of their potential parental melts. The results of our computations show that Cheshmeh-Bid massive chromitites were crystallized from supra-subduction zone melts with boninitic affinity, consistent with the fact that minor and trace elements distributions in the studied chromite match well with that of chromian spinel from boninite lavas. The chromitites would have formed as a result of the reaction of migrating boninitic melts within host peridotite close to the MTZ in a supra-subduction zone setting. Post-magmatic processes (i.e., serpentinization) have only partially obliterated the magmatic fingerprints in some of the chromite grains.

INTRODUCTION

Chromian spinel [$(Mg, Fe^{2+})(Cr, Al, Fe^{3+})_2O_4$] is known to form nearly monomineralic bodies of economic value in the upper mantle section and mantle-crust transition zone of ophiolite complexes (González-Jiménez et al., 2014, for review). The chemistry of chromian spinels in such chromitites can be used as a guide to discriminate between Mid-Ocean Ridge (MOR) and Supra-Subduction Zone (SSZ) settings (Dick and Bullen, 1984; Parkinson and Pearce, 1998; Pearce et al., 2000; Arai et al., 2006a), via the inference of their parental-melt composition and degree of partial melting of their potential mantle source. In their review on the genetic models for the formation of ophiolitic chromitites González-Jiménez et al. (2014) showed that the mechanism by which large volumes of chromian spinel precipitate to form chromitite has long been a controversial topic. Some of the proposed models include: (1) fractional crystallization of basaltic melts followed by mechanical separation within open conduits in the upper mantle or near the mantle-crust transition zone (Dickey, 1975; Greenbaum, 1977; Lago et al., 1982; Leblanc and Ceuleneer, 1992; Leblanc and Nicolas, 1992); (2) mixing or mingling of basaltic melts with different provenance and SiO_2 contents within dunite channels (Paktunc, 1990; Arai and Yurimoto, 1994; Zhou et al., 1994; 1998; 2001; Arai and Abe, 1995; Arai, 1997; Ballhaus, 1998; Gervilla et al., 2005; González-Jiménez et al., 2011; Shi et al., 2012); (3) assimilation of pre-existing mafic rocks by peridotitic intrusions (Bédard and Hébert, 1998; Proenza et al., 1999; Arai et al., 2004; Borisova et al., 2012); (4) segregation of water-rich fluids from small fractions of evolving hydrous and chromite-olivine saturated basaltic melt (Gervilla et al., 2002; González-Jiménez et al., 2011) with important changes in fO_2 or degree of polymerization in the melt (McElduff and Stumpfl, 1991; Melcher et al., 1997; Proenza et al., 1999; Edwards et al., 2000); (5) extensive melt/rock (peridotite) interaction and subsequent melt-mantle mixing within conduits in the upper mantle close to the Moho transition zone (e.g., Zhou et al., 1994; Zhou et al., 1996; Zhou et al., 1998; Grieco et al., 2004; Merlini et al., 2011).

In the last decade, the technique of *in-situ* laser-ablation inductively-coupled plasma-mass spectrometry (LA-ICP-MS) in combination with electron microprobe (EMP) has been widely used to analyze a comprehensive suite of major, minor and trace elements (e.g., Ga, Ti, Ni, Zn, Co, Mn, V and Sc) present in chromite in order to obtain information about their petrogenesis (Dare et al., 2009; Pagé and Barnes, 2009; Aldanmaz, 2012; González-Jiménez et al., 2011; 2014; 2015; Colás et al., 2014). In this contribution, we present the first data on major-, minor- and trace-elements (Ga, Ti, Ni, Zn, Co, Mn, V and Sc) in chromites from podiform chromitites from the Cheshmeh-Bid deposit in the Khajeh-Jamali ophiolite. We use these data to estimate the composition of the magma from which the chromitites formed, as well as the geodynamic environment of their formation. Such information was filtered from the effects of serpentinization and metamorphism on the Cr-spinel composition to ensure that pristine compositions were the only ones used.

GEOLOGICAL SETTING

The Iranian ophiolites belong to the Tethyan ophiolite belt of the Middle East. They have been geographically divided into four groups (Fig. 1a) (Takin, 1972; Stocklin, 1974; McCall, 1985; 1997, and personal communication) namely, (i) ophiolites of northern Iran, considered as remnants of the Paleo-Tethys Ocean (e.g., Alavi, 1991; Saccani et al., 2013a); (ii) ophiolites of the Zagros Suture Zone, including Neyriz and the Kermanshah ophiolites, that are a remnant of the Neo-Tethys Ocean (e.g., Ghazi and Hassanipak, 1999; Nadimi, 2002; Allahyari et al., 2010; Saccani et al., 2013b, 2014; Shafaii Moghadam et al., 2013); (iii) ophiolites of the Makran region, located south of the Sanandaj-Sirjan Zone, and including non-fragmented complexes such as Sorkhband (e.g., Ghazi et al., 2004) and (iv) ophiolites enclosed as tectonic blocks in the Late Cretaceous coloured mélange along the main boundaries of the Central Iranian Micro-continental Block (e.g., Tirrul et al., 1983; Shojaat et al., 2003; Fotoohi Rad et al., 2005; Saccani et al., 2010; Zarrinkoub et al., 2012; Omrani et al., 2013). The Khajeh-Jamali area, which belongs to the second group, includes four ophiolitic massifs in the Zagros Mountain in southwestern Iran, cropping out north of Tashk Lake, about 20 km from the Main Zagros Thrust (Fig. 1a). The Khajeh-Jamali massifs in the study area (Fig. 1b) are mainly composed of mantle harzburgite-dunite tectonite including a Moho transition zone (MTZ) (Rajabzadeh, 1998; Rajabzadeh and Moosavinasab, 2012; Rajabzadeh and Nazari-Dehkordi, 2013; Rajabzadeh et al., 2013). The mantle section consists of homogenous harzburgite alternating with dunite. The crustal section comprises a thick massive serpentinized dunite located at the MTZ, overlain by basaltic pillow lavas associated with radiolarian cherts and Late Cretaceous pelagic limestones. In the northeastern part of the area, limestones of the Jahrom Formation (Eocene-Oligocene) directly overlie the ophiolitic units. In the western part of the area, the ophiolite is tectonically emplaced onto the Late Cretaceous shallow-marine Sarvak Formation. Chromitite bodies of variable size occur at different levels within the mantle harzburgite section and the MTZ of the Khajeh-Jamali massifs.

Most of the chromitite deposits in these massifs, including Cheshmeh-Bid, Khajeh-Jamali, Rajoni and Roni deposits, are in the uppermost part of the mantle section, just at the MTZ or below the petrologic Moho, whereas others, including Neypik and Barandaz deposits, are located in a deeper part of the mantle section (Rajabzadeh, 1998). Some small ore bodies occur in the lower part of the crustal section in cumulitic dunite (Rajabzadeh, 1998); these disseminations are of lesser economic importance. Chromitite pods of this massif have relatively sharp contacts with the enclosing dunite of the Mantle Transition Zone. The Cheshmeh-Bid chromitite mine exploits the largest deposit in the Khajeh-Jamali massifs; it has a tabular shape 0.5 to 8 m thick, 35-50 m wide, and up to 450 m long (including 120,000 tons of ore) which is traversed by shear zones and shows deformation. Chromitites show a wide range of primary textures; these are predominantly massive (Fig. 2a), but semi-massive disseminated ores (Fig. 2b) are common near the contacts with the enclosing dunite. Very rare varieties of microstructures include banded (Fig. 2c) and nodular chromitites (Fig. 2d).

SAMPLING AND ANALYTICAL METHODS

Forty chromitite samples were collected from dumps close to the old mining works; some samples were also collected *in situ* from the unexploited walls at various levels of the Cheshmeh-Bid chromitite mine. Also, two samples from dunite envelope of these chromitites were collected. Thirty polished sections were prepared from a selection of these samples and were studied under reflected light at the Tarbiat Modares University, Iran and by Scanning Electron Microscopy (SEM) at the Department of Earth Sciences

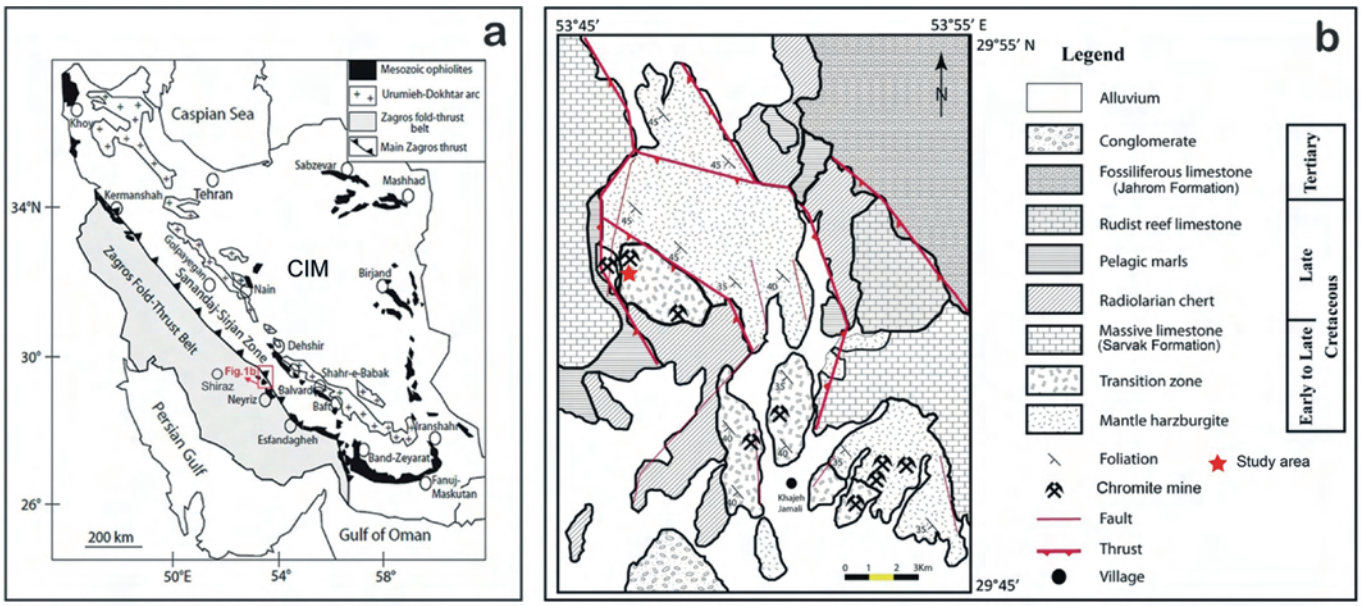

Fig. 1 - a. Map of Mesozoic ophiolites of Iran (Shafaii Moghadam and Stern, 2011), showing the Khajeh-Jamali ophiolitic massifs in the Zagros Suture Zone (area within the rectangle); CIM- Central Iranian Micro-continent. b. Simplified geological map of the Khajeh-Jamali ophiolitic massifs (modified after Rajabzadeh, 1998).

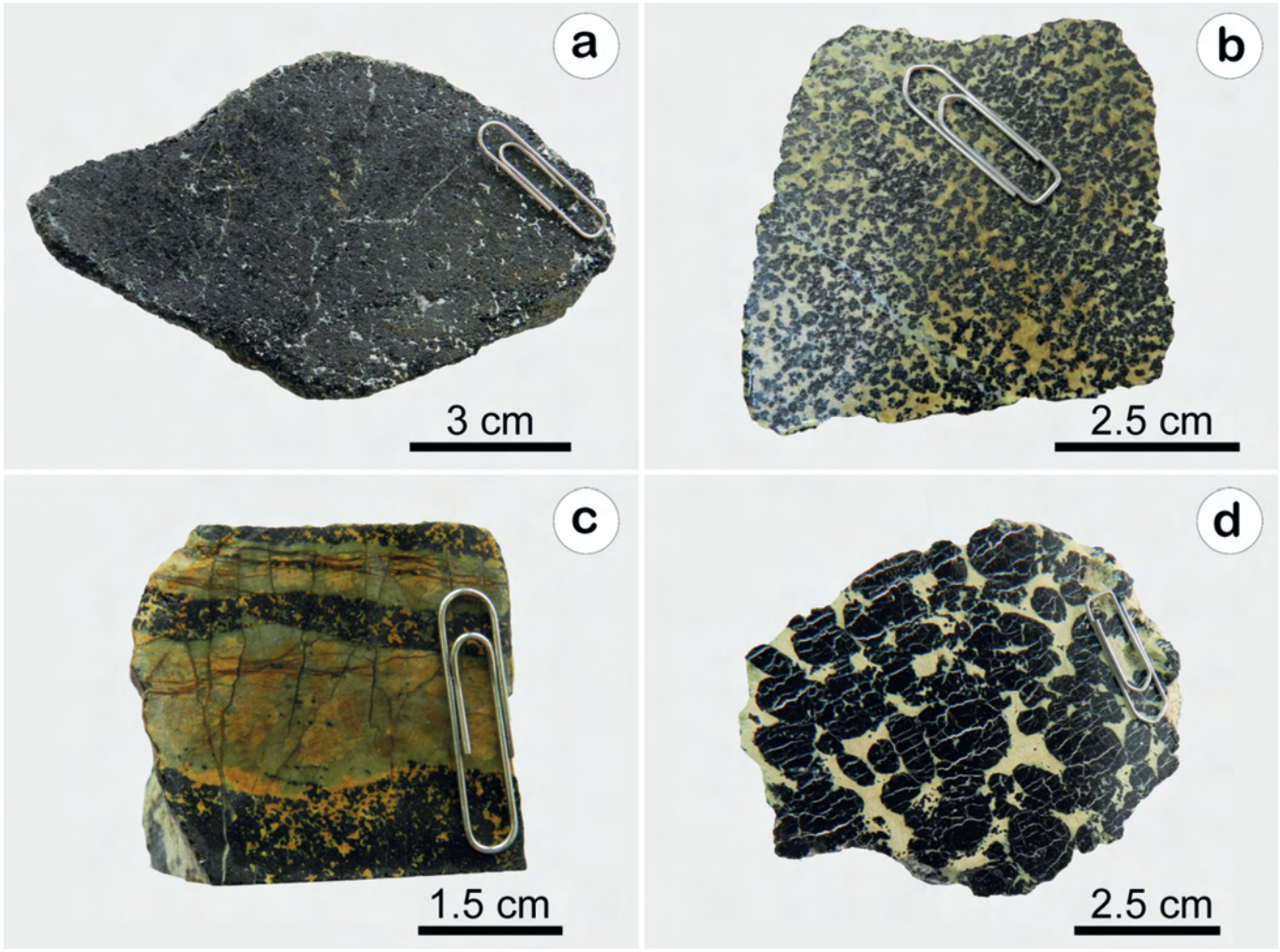

Fig. 2 - Photographs of chromitite textures in Cheshmeh-Bid chromitites: (a) massive, (b) disseminated, (c) banded disseminated, (d) nodular.

(University of Milan, Italy). Chromian spinels were selected for Electron Microprobe analysis (EMPA). Characteristics of samples are shown in Table 1. In order to investigate the alteration of chromian spinels, some altered zones were located on polished sections and then analyzed using a Cambridge Stereoscan electron microscope equipped with an Oxford Link ISIS 300 energy dispersive spectrometer, and an Applied Research Laboratories electron microprobe fitted with six wavelength-dispersive spectrometers and a Tracor Northern energy dispersive spectrometer at the CNR laboratories of Milan. The qualitative analyses were performed at a working distance of 25 mm and an accelerating voltage of 20 kV, while quantitative WDS analyses were obtained at 15 to 25 kV accelerating voltage, 300 nA beam current, and 1 μm beam diameter. The composition of fresh chromites were determined using a Cameca SX100 electron microprobe equipped with five wavelength-dispersive spectrometersat the Geochemical Analysis Unit, GEMOC, Macquarie University, Sydney, Australia. Analyses were performed using a focused beam (1-2 μm) with an accelerating voltage of 15 kV and a beam current of 20-50 nA. The microprobe results are given in Table 2. The trace element concentrations of these chromites were determined by a Photon Machines Excite Excimer 193 nm laser ablation microprobe system coupled to an Agilent 7700 ICP-MS at the Geochemical Analysis Unit, GEMOC, Macquarie University, Sydney, Australia. Ablation was done in a He plus Ar atmosphere with a gas flow of 1.3 L/minute, a repetition rate of 5 Hz, fluence of ~10.6 J cm^{-2} and beam sizes of 50 μm. Raw data were processed on-line using the GLITTER™ software (Version 4.4; Griffin et al., 2008; http://www.glitter-gemoc.com/). The Al content of chromite samples determined by EMP was used as the internal standard for quantification of trace elements.

Due to the small size of altered areas within chromian spinels LA-ICPMS analyses could not be performed and hence trace element compositions are missing.

CHEMICAL CHARACTERISTICS OF THE CHROMIAN SPINELS

Chromitites from the Cheshmeh-Bid podiform chromitite deposit are composed of subhedral to anhedral crystals of chromian spinel in an olivine-serpentine-chlorite groundmass with highly brecciated features. As a first approach, all samples have been tested for alteration and/or metamorphism.

Few samples show medium-reflectivity areas along grain boundaries and within fractures (Fig. 3). Electron microprobe analyses and atomic proportions of cores and rims of chromium spinels from these chromitite samples are given in Table 2. Cores of chromian spinel grains show Cr# [Cr/(Cr + Al)] ranging from 0.70 to 0.85 (average of 0.77) and Mg# [Mg/(Mg + Fe^{2+})] from 0.54 to 0.68 (average of 0.63). The Fe^{3+}# [Fe^{3+}/(Fe^{3+}+ Mg + Al)] of unaltered zones is < 0.05. In contrast, medium-reflectivity areas along boundaries and within fractures display higher Cr# (0.82 to 0.91) with average of 0.86) and lower Mg# (0.44 to 0.70 with average of 0.57). The Fe^{3+}# of these zones is < 0.12. These chromian spinels with medium reflectivity are distinguishable from ferrite-chromite (the common product of low-temperature alteration) by their lower Fe^{3+}#. Fig. 4 shows that cores of chromian spinels from the altered chromitites cluster within the field of the ordinary mantle spinels whereas the high-Cr, high-Fe^{3+} secondary spinels plot in the field of high-Cr spinel, high-Fe^{3+} spinels from the podiform chromitite at Rayat, Iraq (Arai et al., 2006b). Representative microprobe analyses of fresh cores of chromian spinels from the Cheshmeh-Bid chromitites and associated dunites are given in Table 3. Cores of chromian spinels show similar Cr# in disseminated chromitites (0.68-0.82) and semi-massive chromitite with few silicate contents (0.72-0.80), but lower in massive chromitites (0.73-0.74). In contrast, the Mg# is higher in the fresh core of chromian spinel of disseminated and semi-massive (0.60-0.69, 0.62-0.68 respectively) than those from the massive chromitites with Mg# from 0.73 to 0.74. A plot of Cr# versus Mg# (Fig. 5) for studied chromitite samples reveals that increasing of Cr# is coupled with decreasing Mg# from massive to disseminate textures.

Table 1 - Petrographic characteristics of studied chromitites from the Cheshmeh-Bid deposit, Khajeh-Jamali ophiolitic massifs.

Sample No.	Microstructure	Chromite grain zone	Silicate%	Alteration
NCH2A	Semi-massive	Core	ca 4%	Low
NCH2B	Semi-massive	Core	ca 6%	Low
NCH9E	Semi-massive	Core	ca 5%	Low
NCH50	Semi-massive	Core	ca 7%	Low
NCH29	Semi-massive	Core Rim	ca 6%	Low
NCH44	Semi-massive	Core	ca 10%	Low
NCH46	Semi-massive	Core	ca 2-4%	Low
NCH47	Semi-massive	Core Rim	ca 4%	Low
NCH48	Semi-massive	Core	ca 6%	Low
NCH49	Semi-massive	Core Rim	ca 11%	Low
NCH37	Semi-massive	Core	ca 6%	Low
NCH36	Semi-massive	Core	ca 10%	Low
NCH9D	Disseminated	Core	ca 29%	Low
NCH32	Disseminated	Core	ca 35%	Low
NCH27	Disseminated	Core	ca 35%	Low
NCH9B	Disseminated	Core Rim	ca 40%	Low
NCH9A	Massive	Core	0	No
NCH9C	Massive	Core	0	No
NCH9F	Massive	Core	0	No

Minor and trace elements

Minor- and trace-element compositions of fresh cores of chromian spinels from the Cheshmeh-Bid chromitites are given in Table 4. The Zn, Co and Mn contents in chromian spinel are negatively correlated with Mg# (Table 3). Chromian spinel of disseminated and semi-massive chromitites is richer in Zn (424-552 ppm and 408-568 ppm, respectively) than that of massive ones (397-399 ppm). Mn is enriched in chromian spinel of disseminated and semi-massive chromitites (1087-1445 ppm and 1070-1289 ppm) relative to that of massive ones (908-1002 ppm). Chromian spinels of disseminated and semi-massive chromitites are

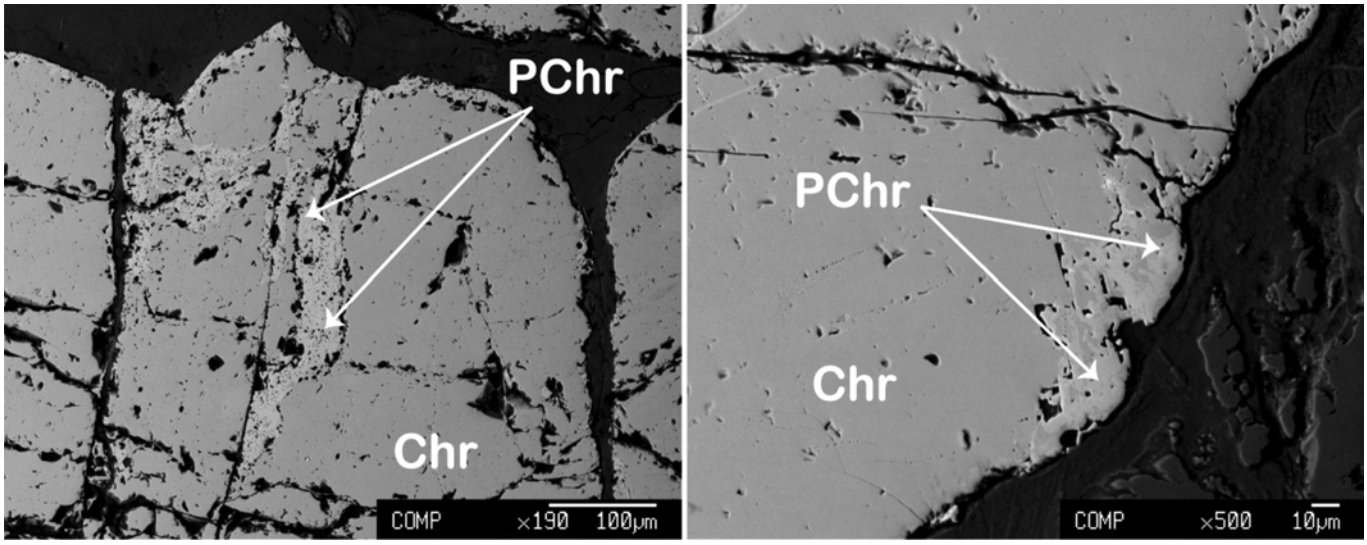

Fig. 3 - Back-Scattered Electron images of porous chromian spinel with medium-reflectivity along grain boundaries and within fractures (PChr- Porous chromite; Chr- Chromite).

Table 2 - Representative microprobe analyses of cores and rims of chromian spinels from the Cheshmeh-Bid chromitites.

Sample No.	NCH9B									NCH47				NCH49				NCH29	
Grain No.	1						2			1		2		1		2		1	
	Core	Rim					Core	Rim		Core	Rim	Core	Rim	Core	Rim	Core	Rim	Core	Rim
Spot No.	n=7	1	2	3	4	6	n=4	1	3	n=10	1	n=5	3	n=6	3	n=4	1	n=3	2
Cr_2O_3	55.14	55.89	53.24	59.2	59.82	57.83	54.21	55.8	55.84	59.60	35.68	61.80	56.85	58.34	58.86	57.85	58.16	63.22	58.79
Al_2O_3	15.11	6.88	6.12	5.78	3.95	5.14	15.54	5.76	8.38	11.47	8.85	8.43	8	12.21	8.76	11.38	6.41	7.82	5.55
TiO_2	0.13	0.14	0.14	0.16	0.15	0.16	0.13	0.15	0.12	0.08	0.06	0.08	0.07	0.08	0.07	0.08	0.08	0.09	0.09
FeO^{total}	14.93	20.52	23.62	17.14	21.23	24.67	15.03	26.87	21.17	15.14	33.19	16.32	21.09	14.45	18.41	15.15	21.41	16.75	16.88
MgO	14.18	10.55	9.53	13.8	10.38	8.42	14.57	9.09	12.46	13.07	13.83	12.05	11.46	13.52	12.28	13.32	12.03	10.99	12.71
MnO	0.18	0.23	0.29	0.26	0.3	0.26	0.16	0.27	0.24	0.16	0.12	0.23	0.16	0.15	0.26	0.18	0.23	0.11	0.2
NiO	0.13	0.19	0.11	0.15	0.21	0.19	0.10	0.11	0.1	0.14	0	0.09	0.14	0.14	0.08	0.09	0	0.09	*BDL*
V_2O_3	0.13	0.11	0.13	0.15	0.13	0.09	0.14	0.14	0.19	0.17	0.1	0.16	0.17	0.19	0.15	0.15	0.16	0.16	0.16
Total	99.88	94.51	93.18	96.64	96.17	96.76	99.87	98.19	98.5	99.83	91.83	99.16	97.94	99.08	98.87	98.20	98.48	99.24	94.38
Formula units based on 4 oxygens																			
Cr	1.380	1.578	1.550	1.613	1.690	1.639	1.354	1.561	1.497	1.524	1.058	1.624	1.539	1.493	1.557	1.502	1.577	1.671	1.644
Al	0.564	0.290	0.266	0.235	0.166	0.217	0.579	0.240	0.335	0.437	0.391	0.330	0.323	0.466	0.346	0.441	0.259	0.308	0.231
Ti	0.003	0.004	0.004	0.004	0.004	0.004	0.003	0.004	0.003	0.002	0.002	0.002	0.002	0.002	0.002	0.002	0.002	0.002	0.002
Fe^{3+}	0.061	0.160	0.229	0.186	0.173	0.174	0.077	0.249	0.210	0.040	0.727	0.051	0.173	0.043	0.120	0.065	0.209	0.017	0.155
Fe^{2+}	0.333	0.452	0.500	0.308	0.462	0.565	0.319	0.546	0.391	0.371	0.315	0.405	0.432	0.349	0.399	0.352	0.408	0.450	0.345
Mg	0.669	0.562	0.523	0.709	0.553	0.450	0.686	0.479	0.630	0.630	0.773	0.597	0.585	0.652	0.612	0.652	0.615	0.547	0.670
Mn	0.005	0.007	0.009	0.008	0.009	0.008	0.004	0.008	0.007	0.004	0.004	0.006	0.005	0.004	0.007	0.005	0.007	0.003	0.006
Ni	0.003	0.004	0.003	0.003	0.005	0.005	0.002	0.003	0.002	0.003	0.000	0.002	0.003	0.003	0.002	0.002	0.000	0.002	0.000
V	0.002	0.002	0.002	0.002	0.002	0.001	0.002	0.002	0.003	0.002	0.002	0.002	0.002	0.002	0.002	0.002	0.002	0.002	0.002
Total	3.415	3.672	3.813	3.561	3.700	3.804	3.422	3.887	3.677	3.423	4.312	3.473	3.668	3.405	3.562	3.440	3.692	3.471	3.556
Mg#	0.67	0.55	0.51	0.7	0.54	0.44	0.68	0.47	0.62	0.63	0.71	0.59	0.57	0.65	0.61	0.65	0.6	0.54	0.66
Cr#	0.71	0.84	0.85	0.87	0.91	0.88	0.70	0.87	0.82	0.78	0.73	0.83	0.83	0.76	0.82	0.78	0.86	0.85	0.88
Fe^{3+}#	0.03	0.08	0.11	0.09	0.09	0.09	0.04	0.12	0.1	0.02	0.33	0.03	0.08	0.02	0.06	0.04	0.1	0.01	0.08
Fe^{2+}#	0.33	0.45	0.49	0.3	0.46	0.56	0.32	0.53	0.38	0.37	0.29	0.41	0.43	0.35	0.39	0.35	0.4	0.46	0.34

Table 3 - Representative microprobe analyses of chromian spinels from the Cheshmeh-Bid chromitites and associated dunites.

	Chromitite																			Serpentinized dunite	
Sample No./IRNCH	2A	2B	9E	50	29	44	46	47	48	49	37	36	9D	32	27	9B	9A	9C	9F	38	43
Number of analyses	n=5	n=5	n=5	n=5	n=4	n=5	n=4	n=4	n=5	n=5	n=5	n=4	n=5	n=5	n=5	n=5	n=5	n=4	n=5	n=5	n=4
Cr_2O_3	56.96	55.73	55.86	59.61	58.20	55.09	55.80	57.42	57.84	56.80	54.90	57.02	57.44	59.79	57.62	51.96	54.44	54.66	55.64	53.89	51.59
Al_2O_3	10.16	12.53	11.69	10.28	10.20	12.16	13.24	11.84	10.98	13.79	14.11	11.82	10.59	8.94	10.53	16.40	13.35	13.13	13.20	12.66	14.01
TiO_2	0.08	0.08	0.07	0.08	0.08	0.08	0.08	0.08	0.08	0.07	0.10	0.08	0.10	0.07	0.09	0.12	0.09	0.11	0.11	0.06	0.00
FeO^{total}	17.22	14.64	16.44	14.77	16.15	15.13	15.75	15.68	15.38	14.42	15.05	16.43	16.49	17.72	17.68	14.39	12.97	13.12	13.21	21.69	22.54
MgO	12.43	13.84	12.79	12.65	12.92	13.64	13.10	13.11	13.04	13.99	14.17	13.29	12.44	12.18	12.49	14.51	15.23	15.13	15.27	10.42	9.05
MnO	0.19	0.14	0.16	0.15	0.16	0.16	0.17	0.17	0.15	0.14	0.15	0.17	0.20	0.20	0.19	0.15	0.14	0.11	0.13	0.26	0.28
NiO	0.12	0.15	0.14	0.14	0.17	0.07	0.15	0.14	0.13	0.15	0.16	0.04	0.14	0.00	0.00	0.11	0.16	0.16	0.17	0.00	0.03
V_2O_3	0.22	0.13	0.20	0.19	0.18	0.16	0.19	0.16	0.18	0.17	0.16	0.20	0.16	0.20	0.25	0.13	0.15	0.16	0.16	0.22	0.39
Total	97.38	97.24	97.34	97.82	97.93	96.50	98.47	98.58	97.69	99.52	98.81	99.04	97.44	99.11	98.90	97.77	96.53	96.58	97.89	99.19	97.88
Formula units based on 4 oxygens																					
Cr	1.514	1.449	1.468	1.562	1.529	1.448	1.436	1.485	1.513	1.435	1.396	1.471	1.516	1.573	1.506	1.316	1.408	1.415	1.422	1.414	1.371
Al	0.403	0.486	0.458	0.402	0.399	0.477	0.508	0.457	0.428	0.519	0.535	0.455	0.417	0.351	0.411	0.620	0.515	0.507	0.503	0.495	0.555
Ti	0.002	0.002	0.002	0.002	0.002	0.002	0.002	0.002	0.002	0.002	0.002	0.002	0.003	0.002	0.002	0.003	0.002	0.003	0.003	0.001	0.000
Fe^{3+}	0.100	0.076	0.086	0.035	0.083	0.090	0.062	0.065	0.066	0.050	0.079	0.088	0.076	0.092	0.098	0.073	0.090	0.090	0.086	0.111	0.088
Fe^{2+}	0.386	0.327	0.372	0.375	0.366	0.331	0.368	0.364	0.360	0.336	0.326	0.361	0.385	0.404	0.392	0.311	0.264	0.267	0.270	0.495	0.554
Mg	0.623	0.678	0.634	0.625	0.640	0.676	0.636	0.639	0.643	0.666	0.679	0.646	0.619	0.604	0.616	0.693	0.743	0.739	0.736	0.515	0.453
Mn	0.005	0.004	0.005	0.004	0.005	0.005	0.005	0.005	0.004	0.004	0.004	0.005	0.006	0.006	0.005	0.004	0.004	0.003	0.004	0.007	0.008
Ni	0.003	0.003	0.003	0.003	0.004	0.002	0.003	0.003	0.003	0.003	0.003	0.001	0.003	0.000	0.000	0.002	0.003	0.003	0.004	0.000	0.001
V	0.002	0.002	0.003	0.003	0.002	0.002	0.002	0.002	0.002	0.002	0.002	0.003	0.002	0.003	0.003	0.002	0.002	0.002	0.002	0.003	0.005
Total	3.522	3.430	3.488	3.421	3.478	3.453	3.451	3.453	3.448	3.403	3.432	3.479	3.488	3.526	3.523	3.410	3.387	3.389	3.386	3.644	3.668
Mg#	0.62	0.68	0.63	0.62	0.64	0.67	0.63	0.64	0.64	0.66	0.68	0.64	0.62	0.60	0.61	0.69	0.74	0.74	0.73	0.51	0.45
Cr#	0.79	0.75	0.76	0.80	0.79	0.75	0.74	0.77	0.78	0.74	0.72	0.76	0.78	0.82	0.79	0.68	0.73	0.74	0.74	0.74	0.71
Fe^{3+}#	0.05	0.04	0.04	0.02	0.04	0.04	0.03	0.04	0.03	0.02	0.04	0.05	0.04	0.05	0.05	0.03	0.05	0.05	0.04	0.06	0.04
Fe^{2+}#	0.38	0.33	0.37	0.38	0.36	0.33	0.37	0.37	0.36	0.34	0.32	0.36	0.38	0.40	0.39	0.31	0.26	0.27	0.27	0.49	0.55

Table 4 - Minor- and trace-element compositions (in ppm) of chromian spinels from the Cheshmeh-Bid chromitites and associated dunites.

	Chromitite																Serpentinized dunite	
IRNCH	2A	2B	9E	50	29	44	46	47	48	49	37	36	9D	32	27	9B	9A	9C	9F	38	43
Number of analyses	n=5	n=5	n=5	n=5	n=5	n=5	n=4	n=4	n=5	n=5	n=5	n=4	n=5	n=5	n=5	n=5	n=5	n=4	n=5	n=5	n=4
Sc	7	6	7	7	7	6	6	7	7	6	5	6	6	6	7	6	6	5	6	5	6
Ti	486	470	445	468	530	512	507	504	471	493	594	471	612	448	537	735	652	637	650	378	131
V	776	1323	1052	994	941	892	925	882	1031	921	892	1012	798	1162	1262	684	856	846	849	1138	1956
Mn	1112	1281	1225	1183	1153	1134	1218	1289	1146	1070	1077	1171	1256	1445	1349	1087	1002	908	912	1790	1871
Co	176	196	191	197	192	183	183	188	181	178	179	175	213	223	211	188	169	165	165	369	376
Ni	911	754	771	690	701	851	922	887	819	916	1057	733	615	442	611	831	1185	1285	1156	379	487
Zn	415	568	516	408	455	465	470	503	498	456	488	459	426	534	552	424	398	399	397	1560	1963
Ga	22	21	21	19	19	22	23	22	21	24	24	20	19	17	20	27	23	22	22	18	21

Fig 4 - Ternary Cr-Al-Fe^{3+} plot of chromian spinel in Cheshmeh-Bid podiform chromitites. Fresh and altered zones of chromian spinels are shown by filled and open symbols, respectively. Fields of mantle chromitites (Arai and Yurimoto, 1994) and high Cr# spinels of chromitites from Rayat (Iraq) (Arai et al., 2006b) are shown for comparison.

Fig. 5 - Cr# [Cr/(Cr+Al)] versus Mg# [Mg/(Mg+Fe^{2+})].

also higher in Co (188-223 ppm and 175-197 ppm, respectively) than those of massive chromitites (165-169 ppm). Ni and Sc correlate negatively with Cr# (Table 3). Ni increases from 442 to 831 ppm in disseminated, to 690-1057 ppm in semi-massive, and to 1156-1285 ppm in massive chromitites. Ti contents of high-Cr cores of chromian spinels in the massive chromitites range from 637 to 652 ppm, from 445-594 ppm in semi-massive and from 445 to 735 ppm in disseminated chromitites. Sc and Ga contents of these chromitites are low and do not show correlation with Cr# and Mg# in the different chromitite textures (Table 3).

DISCUSSION

Parent melt composition and tectonic discrimination

High-Cr, low-Fe^{3+} spinel along the cracks and margins of chromite grains from the Cheshmeh-Bid chromitites is perhaps the strongest evidence that studied chromitites are affected by post-magmatic alteration. Presence of chromian spinels with high-Cr and low Fe^{3+} within chromitites has been pointed out by several authors (e.g., Arai et al., 2006b; Gervilla et al., 2012). This chemical feature is widely attributed to subtraction of Al as chlorite with the addition of minor amounts of Fe from interstitial silicates. Arai et al. (2006b) suggested that high-Cr and low-Fe^{3+} in chromian spinels of Rayat chromitites from the Northeastern Iraq may indicate a composition on a limb of solvus at this high-Cr, low-Fe^{3+} chemical condition (e.g., Sack and Ghiorso, 1991). Gervilla et al. (2012) suggested that ferrian chromite can be formed in a two-stage process during the retrograde evolution of chromitites. During the first stage, primary chromite may reacts with olivine in the presence of reducing fluids to produce chlorite and secondary chromite with porous texture enriched in Cr_2O_3 and Fe^{2+}. In the second stage, late oxidizing hydrothermal solutions percolate through pores in the porous chromite, dissolving chlorite and adding Fe^{3+} to the chromite and formed Fe^{3+}-rich chromite.

The trend shown in Fig. 5 might be due to subsolidus re-equlibrium and/or alteration. Subsolidus re-equilibration between chromite and an interstitial silicate phase (most typically olivine) would change chromite composition from its original composition. Despite of this fact, the primary geochemistry of chromian spinels in massive chromitites, with more than 90% chromite modal composition, will be preserved during low temperature re-equilibration processes (e.g., Maurel and Maurel, 1982). Thus, only massive chromitites which are not or slightly affected by subsolidus re-equilibration have been used for assessing the origin of the parental magma and tectonic discrimination. The chromites from the Cheshmeh-Bid massive chromitites have Cr_2O_3 contents in the range of 54.4-59.6 wt%, Al_2O_3 contents in the range of 10.2-14.1 wt% and TiO_2 contents 0.07 to 0.11 wt% which are consistent with composition of typical ophiolitic podiform chromitites (Fig. 6a and b). The studied fresh chromites are typical of podiform chromitites, as shown on Fig. 7. The Cr# extends from the high-Cr# boninite field to the low-Cr# MORB field. The studied spinels have compositions similar to high-Cr spinels from the Albanian podiform chromitites but with lower Fe^{2+}# (Beccaluva et al., 1998; Saccani and Tassinari, 2015) and ophiolites of Sarve-Abad (Allahyari et al., 2014), Turkey (Paktunc and Cabri, 1995), Troodos (Arai and Yurimoto, 1994), northern Oman-United Arab Emirates (UAE) (Arai and Yurimoto, 1994) (Fig. 7). In order to decipher the geological setting of the Cheshmeh-Bid chromitites, geological setting of the chromitite xenoliths from the Japan arc as suprasubduction zone (Arai and Abe, 1994) and chromitites of the Hess Deep as mid-ocean ridge setting (Arai and Matsukage, 1998) have also been plotted in Fig. 7.

Linear relationships between the Al_2O_3 and TiO_2 content of chromite and the parental melt composition have been experimentally established (Maurel and Maurel, 1982), as well as through the study of natural systems (Roeder and Reynolds, 1991; Kamenetsky et al., 2001). Kamenetsky et al. (2001) used chromite-olivine pairs and melt inclusion-chromite pairs from various tectonic settings such as oceanic, arc and intraplate tectonic settings. Thus, calculated Al_2O_3 and TiO_2 compositions of parental melts can be used to infer the magmatic affinity of the parental melt, as well as the tectonic setting of formation of the chromitite. Al_2O_3 and TiO_2 contents in chromite have used to estimate the geochemical composition of a melt from which the chromite crystallised (Pagé and Barnes, 2009). The Al_2O_3 and TiO_2, chromite-parent melt composition relationship has been applied to the chromites of the Cheshmeh-Bid chromitites. For this point, we have used the Al_2O_3 and TiO_2 chromite-parent melt composition relationship from natural sample suites of Kamenetsky et al. (2001) using equations (1) and (2). The Al_2O_3 contents of the parental melts have been calculated using the following equation:

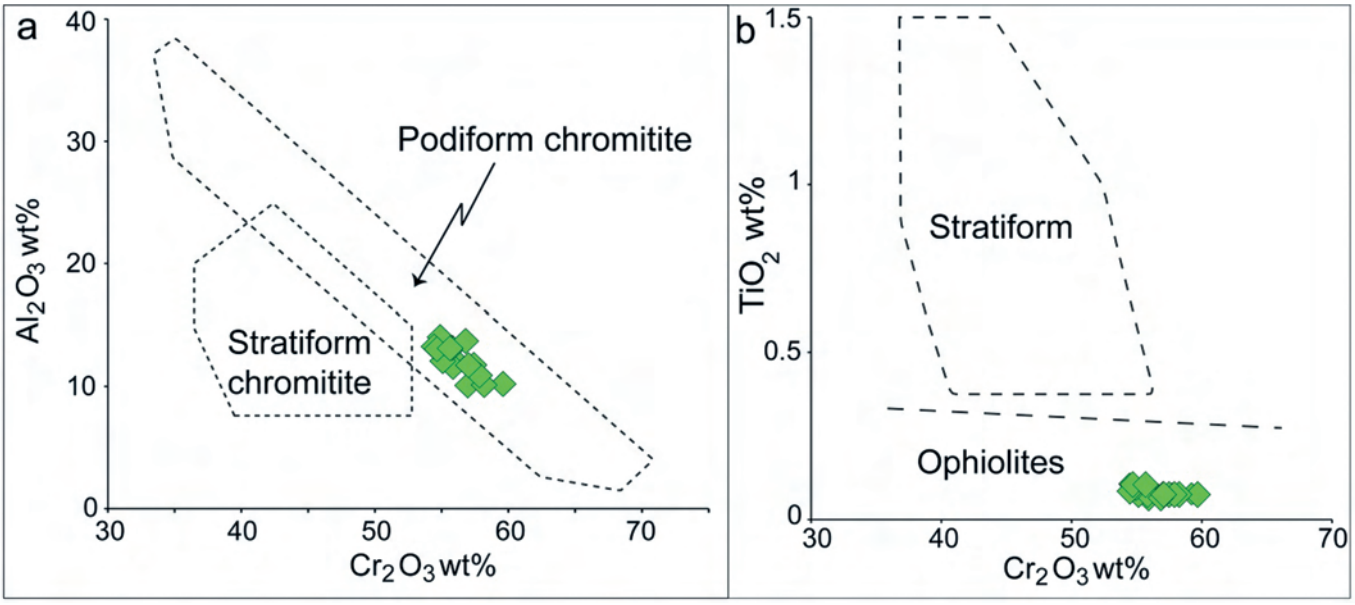

Fig. 6 - Compositional variations of Cheshmeh-Bid chromitites: (a) Cr_2O_3 versus Al_2O_3 (wt%). (b) Cr_2O_3 versus TiO_2 (wt%); The fields for podiform and stratiform chromitites are from Arai et al. (2004).

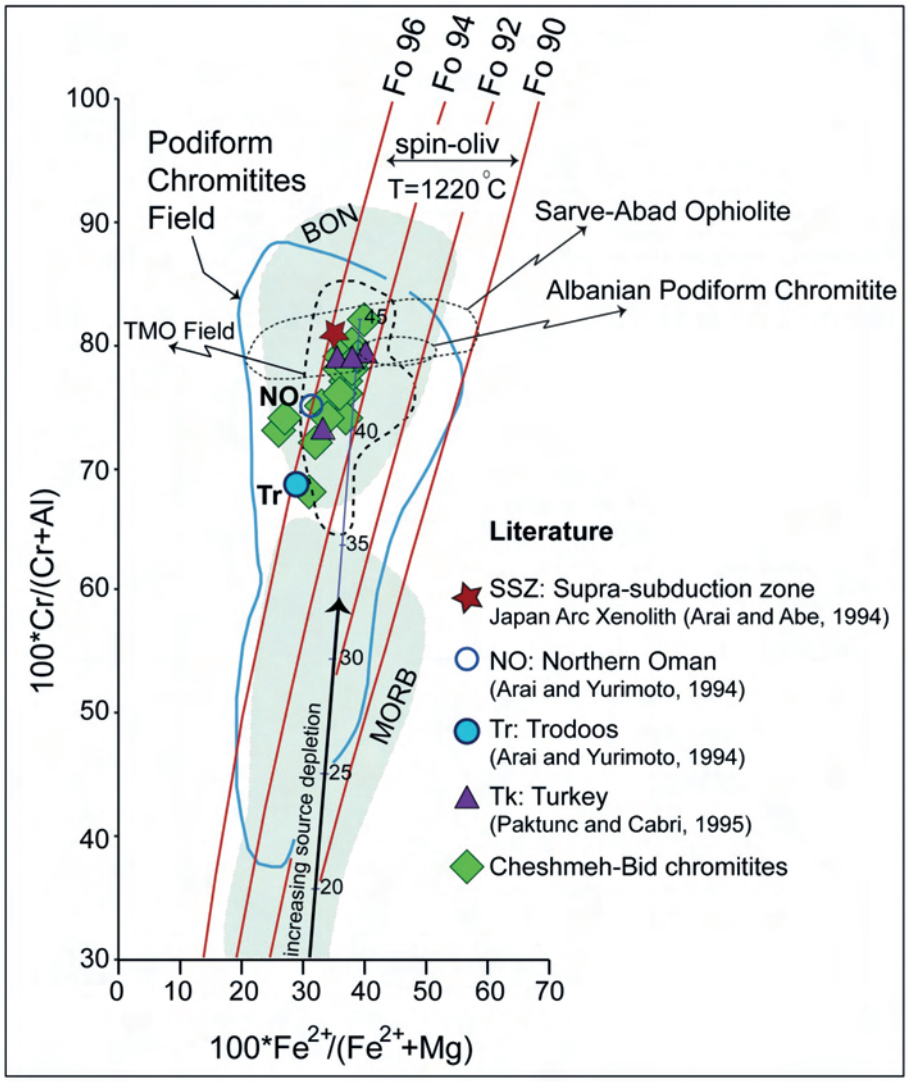

Fig. 7 - Compositional variations of Cr# (100*Cr/(Cr + Al)) versus Fe^{2+}# (100*Fe^{2+}/(Fe^{2+} + Mg)) in chromian spinels of the Cheshmeh-Bid chromitites (diamonds). Compositional fields of mid-ocean ridge basalt (MORB) and boninite (BON) are from Barnes and Roeder (2001). The spinel-olivine re-equilibration curves (spin-oliv) at 1220°C are from Dick (1977). Fields of Albanian Podiform Chromitites (Beccaluva et al., 1998; Saccani and Tassinari, 2015), chromitites of Sarve-Abad ophiolite (Allahyari et al., 2014) and podiform chromitites (Pagé and Barnes, 2009) are shown for comparison. Data of podiform chromitite from Northern Oman (NO; Arai and Yurimoto, 1994), Trodoos (Tr; Arai and Yurimoto, 1994), Turkey (Tk; Paktunc and Cabri, 1995) and a suprasubduction zone (SSZ) nodular-textured chromitite xenolith from the Japan arc (Arai and Abe, 1994) are shown for comparison.

$$\text{wt \% } Al_2O_3 \text{ in melt} = 5.0258 \cdot [ln(\text{wt \% } Al_2O_3 \text{ in spinel})] - 0.6867 \quad (1)$$

Similarly, it is possible to calculate the TiO_2 content of the parental melt by using the following equation which has been applied for low-Al chromian spinels:

$$\text{wt\% } TiO_2 \text{ in melt} = 1.112 \cdot (\text{wt\% } TiO_2 \text{ in spinel})^{0.7893} \quad (2)$$

In this part, TiO_2 and Al_2O_3 contents of parental melt in equilibrium with the Cheshmeh-Bid chromitites data were calculated based on data from Kamenetsky et al. (2001), and equations (1) and (2). Position of chromitite samples on the regression lines related to the arc lavas is shown in Fig. 8.

The calculated Al_2O_3 contents of melt vary from 10.97 to 12.62 wt%. The calculated TiO_2 contents ranges from 0.14 to 0.19 wt%. These values are consistent with TiO_2 and Al_2O_3 contents of boninites from several localities such as Thetford Mines Ophiolite (Pagé and Barnes, 2009), Betts Cove (Bédard, 1999), Chichijima (Taylor et al., 1994), Dinaride ophiolites (Dilek et al., 2008; Saccani et al., 2008; 2011) (Fig. 9). The FeO/MgO ratio of the parent melt was calculated from the chromite composition by equation (3) which has been proposed by Maurel and Maurel (1982):

$$\ln(FeO/MgO)_{spinel} = 0.47\text{-}1.07Y^{Al}_{spinel} + 0.64Y^{Fe+3}_{spinel} + \ln(FeO/MgO)_{melt} \quad (3)$$

where

$$Y^{Al}_{spinel} = Al/(Cr + Al + Fe^{+3})$$

and

$$YFe^{+3} \text{ spinel} = Fe^{+3}/(Cr + Al + Fe^{+3}).$$

Post-magmatic subsolidus re-equilibration would trigger exchange of Mg^{2+} and Fe^{2+} cations between chromite and olivine. As discussed above, only massive chromitites have been used to estimate FeO/MgO ratio of parental melt as they underwent minimal subsolidus Fe-Mg exchange between their chromite and interstitial silicates. The FeO/MgO ratios of the parental melt of studied chromitite range between 0.68 and 1.04 which reflects boninite chemistry of parental melt (Hichey and Frey, 1982; Fallooon and Crawford, 1991; Saccani et al., 2011; Saccani and Tassinari, 2015). The FeO/MgO ratios and TiO_2, Al_2O_3 concentrations in parental melts of the Cheshmeh-Bid chromitite is similar to boninitic parental melts which has been inferred from chromian spinel composition in other Late Cretaceous Zagros ophiolites (e.g., Penjween-Walash ophiolites of the

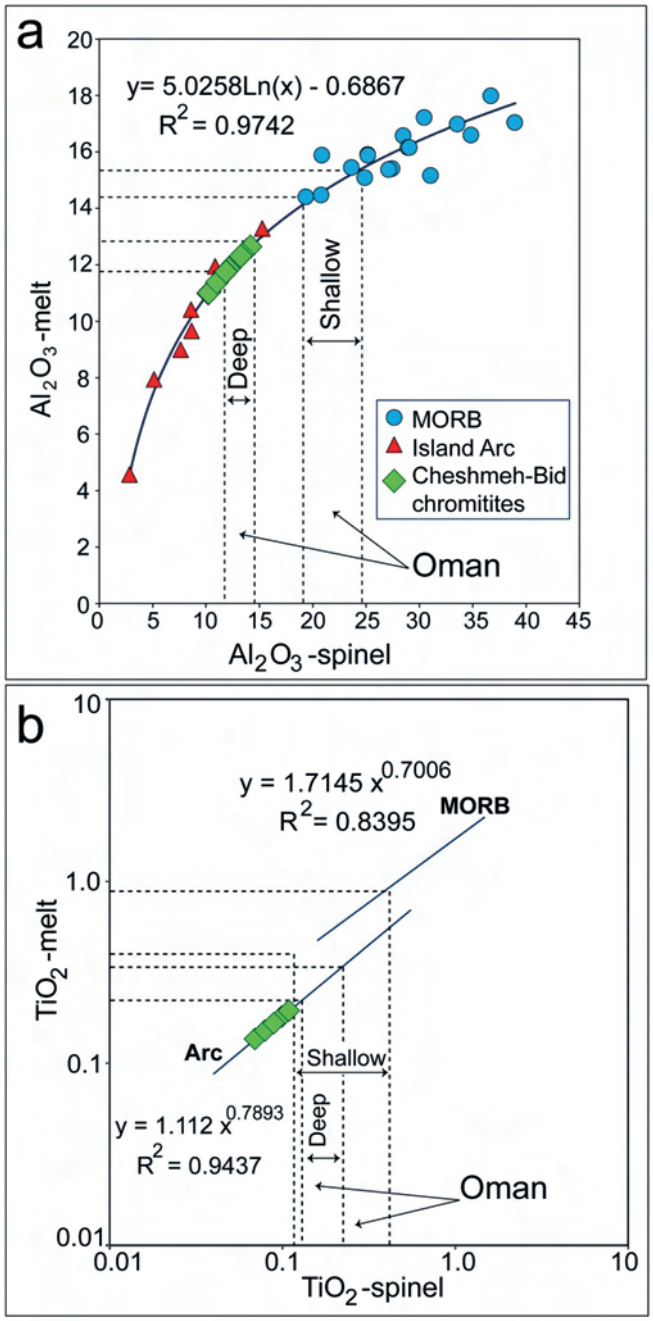

Fig. 8 - Al_2O_3 (a) TiO_2 (b) melt-spinel relationship for the studied chromian spinels, after Kamenetsky et al. (2001). The spinel compositions from the shallow and deep Wadi Rajmi (Oman) chromitites and the calculated melt compositions (Rollinson, 2008) are included for comparison. MORB-Mid-Ocean Ridge Basalt.

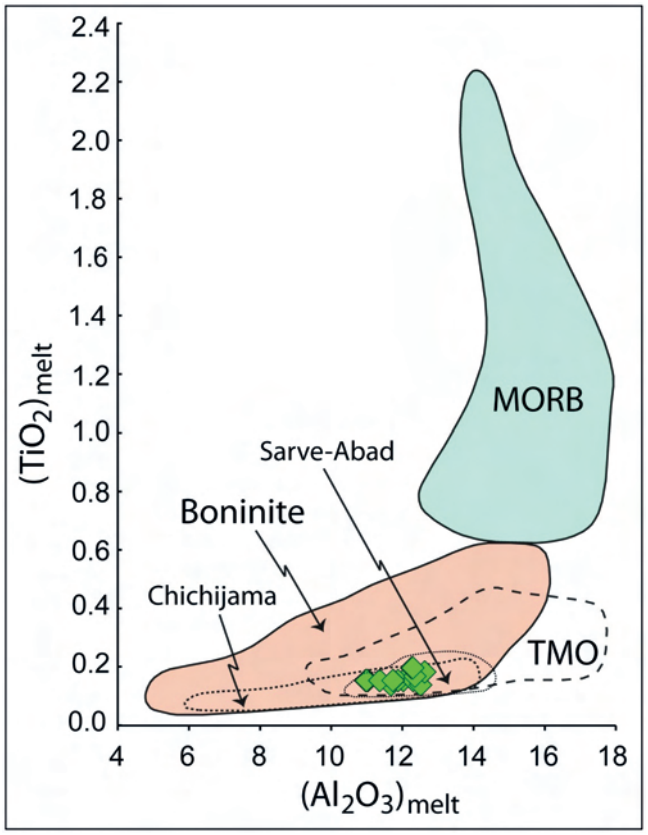

Fig. 9 - TiO_2 (wt%) versus Al_2O_3 (wt%) compositions of melt calculated to be in equilibrium with chromian spinels from the Cheshmeh-Bid chromitite deposit. The fields of Thetford Mines Ophiolite, boninites and MORB are from Page and Barnes (2009). Fields of Chichijama boninites (Taylor et al., 1994) and Sarve-Abad chromites (Allahyari et al., 2014) are shown for comparison.

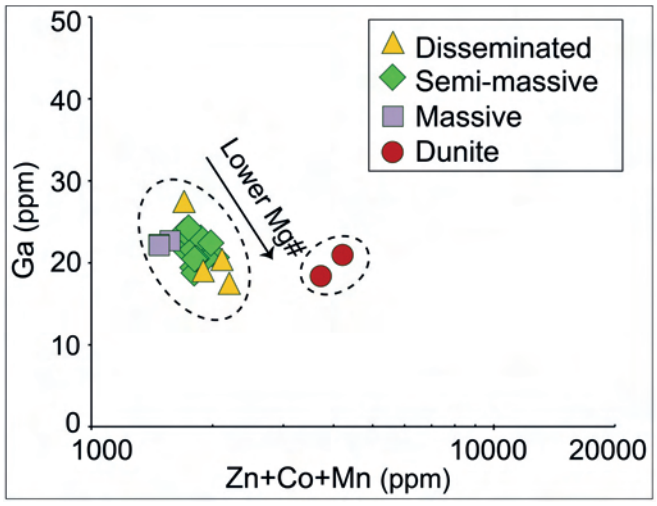

Fig. 10 - Zn+Co+Mn (ppm) versus Ga (ppm) of chromites from the Cheshmeh-Bid chromitite (after Colás et al., 2014).

northwestern Zagros Suture Zone in Kudristan of Iraq, Aswad et al., 2011; Sarve-Abad ophiolites of northwestern Iran, Allahyari et al., 2014; Gogher-Baft ophiolites of southeastern Iran, Shafaii Moghadam et al., 2013).

Trace and minor element compositions as proxy for chromitite genesis

The application of trace elements in chromian spinels of chromitites to infer the genesis of podiform chromitites, has been described by Pagé and Barnes (2008). It is crucial to note that minor elements in pristine cores of chromian spinels might be perturbed due to post-magmatic re-equilibration processes (González-Jiménez et al., 2011; Colás et al., 2014). Most of the Cheshmeh-Bid chromitites were not affected by intense hydrothermal alteration. The plot of Ga versus Zn + Co + Mn for all studied chromitites (Fig. 10) shows that as Mg# decreases, there is a similar negative cor-

relation between Ga and Zn + Co + Mn from massive to disseminated chromitites. Slight enrichment of trace elements like Zn, Co and Mn in most of massive chromitites as well as disseminated chromitites may reflect the post-magmatic sub-solidus re-equilibration with olivine matrix. Colás et al. (2014) observed similar enrichment in unmetamorphosed chromites of disseminated samples from chromitite dyke of Dyne in New Caledonia Ophiolite. They suggested that Mn, Zn and Co, together with Fe^{2+}, can enter the tetrahedral sites after Mg^{2+} sequestration into olivine during cooling and subsolidus re-equilibration between chromite and olivine. Dunite samples of the Cheshmeh-Bid massif with strong enrichment of Zn + Co + Mn show how dunite with high silicate/chromite ratio can be affected by subsolidus re-equilibration during cooling.

In summary, trace and minor element compositions of chromian spinels from massive chromitite can be used as proxy for chromitite genesis, provided that they are not affected by subsolidus re-equilibration and/or hydrothermal alteration. Spider-diagrams of major, minor and trace elements

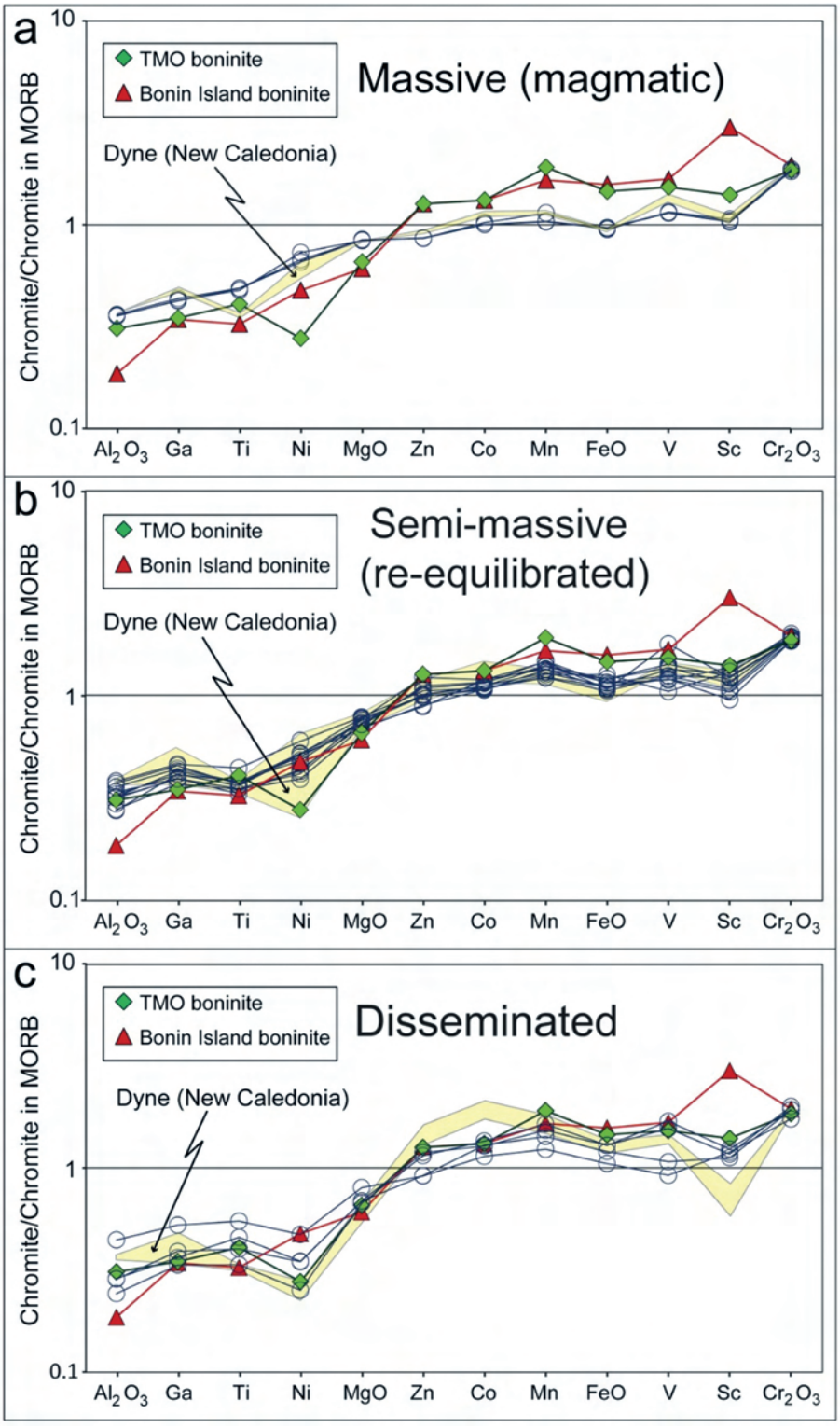

Fig. 11 - Spidergrams showing the composition of chromites from the Cheshmeh-Bid massive (a), semi-massive (b) and disseminated (c) chromitites compared with chromites from boninites (Bonin Island and the Thetford Mines Ophiolite, Page and Barnes, 2009) normalized to the composition of chromites from the MORB. Normalizing values of MORB are from Page and Barnes (2009). Data for chromitites of Dyne in the New Caledonia Ophiolite are also from Colás et al. (2014).

from massive, semi-massive and disseminated chromitites (Fig. 11) are normalized to the composition of chromite from East Pacific Rise MORB. The patterns of minor and trace elements in chromian spinels of the Cheshmeh-Bid chromitites are also similar to those of high-Cr chromites from the Dyne chromitites of New Caledonia Ophiolite. Disseminated chromitites of Dyne are more enriched in Zn, Co and Mn than those from the Cheshmeh-Bid chromitites which means that they are more re-equilibrated than Cheshmeh-Bid chromitites. Chromian spinels of massive and re-equilibrated semi-massive chromitites show patterns similar to Thetford Mines Ophiolite with small changes such as slight enrichment of Zn-Mn-Co in re-equilibrated chromitites and Sc negative anomaly. Similarity with Thetford mine chromitites suggests that chromian spinels from the Cheshmeh-Bid chromitites crystallised from a boninitic melt while discrepancy with Bonin lava spinels can be due to their low chromite to silicate ratio and higher degree of re-equilibration.

Mantle oxidation state

The oxidation state of the mantle can be affected by recycling and accreting processes like subduction and flux of oxidized crustal components into a moderately reduced, poorly buffered asthenosphere (Ballhaus et al., 1990). Thus it is not surprising that oxygen fugacity has been found to vary widely across a range of tectonic settings. It has been suggested that subduction zone settings are more highly oxidized than other tectonic settings (e.g., Ballhaus et al., 1990; Parkinson and Arculus, 1999). One way to approach the oxidation state of the mantle is the application of olivine-spinel oxygen barometer of Ballhaus et al. (1991a and 1991b). It is crucial to note that no orthopyroxene has been found in podiform chromitites and associated dunites, and only coexisting olivine-chromian spinel pairs are available for such calculations. Representative electron microprobe analyses of olivine-chromian spinel pairs are given in Table 5. The calculated oxygen fugacities of two massive chromitites, three disseminated chromitites and one dunite sample are given in Table 6. The calculated f_{O2} values of the studied samples are above the FMQ buffer and plot into the field of oceanic-arc peridotites (Fig. 12).

Table 5 - Representative microprobe analyses of chromite-olivine pairs from the Cheshmeh-Bid chromitites and dunites.

Sample No.	CH210	CH93	H39	CH201	CH202	CH19
Rock type	Massive chromitite		Disseminated chromitite			Dunite
Mineral	Spinel					
TiO_2	0.06	0.10	0.03	0.13	0.09	0.04
Al_2O_3	10.5	13.00	10.07	17.30	17.34	11.23
Cr_2O_3	58.9	57.36	60.80	52.97	52.32	58.52
FeO^{tot}	17.4	15.91	16.31	14.97	17.65	19.04
MnO	0.10	0.04	0.04	0.04	0.02	0.09
MgO	13.0	13.83	13.38	15.14	13.26	12.13
NiO	0.07	0.11	0.09	0.14	0.14	0.09
Total	100.15	100.36	100.75	100.69	100.82	101.14
Formula units based on 4 oxygens						
Ti	0.001	0.002	0.001	0.003	0.002	0.001
Al	0.404	0.490	0.384	0.633	0.641	0.429
Cr	1.520	1.449	1.555	1.300	1.298	1.499
Fe^{3+}	0.097	0.074	0.078	0.078	0.073	0.092
Fe^{2+}	0.378	0.348	0.363	0.305	0.386	0.424
Mn	0.003	0.001	0.001	0.001	0.001	0.002
Mg	0.632	0.659	0.645	0.701	0.620	0.586
Ni	0.002	0.002	0.002	0.003	0.003	0.002
Sum	3.512	3.450	3.471	3.414	3.488	3.552
Mg#	0.63	0.65	0.64	0.69	0.62	0.58
Fe^{2+}#	0.37	0.35	0.36	0.31	0.38	0.42
Cr#	0.79	0.75	0.80	0.67	0.67	0.78
Mineral	Olivine					
SiO_2	41.2	42.01	41.27	41.62	41.46	41.79
FeO	5.29	4.68	7.02	4.82	5.74	6.99
MnO	0.08	0.03	0.10	0.05	0.09	0.14
MgO	52.3	52.70	51.97	53.39	52.50	51.54
CaO	0.00	0.01	0.05	0.03	0.01	0.03
NiO	0.70	0.79	0.38	0.56	0.55	0.43
Cr_2O_3	0.05	0.03	0.05	0.04	0.00	0.05
Total	99.65	100.26	100.83	100.51	100.35	100.96
Formula units based on 4 oxygens						
Si	0.996	1.005	0.993	0.995	0.996	1.002
Cr	0.001	0.001	0.001	0.001	0.000	0.001
Mg	1.884	1.879	1.862	1.901	1.879	1.842
Mn	0.002	0.001	0.002	0.001	0.002	0.003
Fe*	0.107	0.094	0.141	0.096	0.115	0.140
Ca	0.000	0.000	0.001	0.001	0.000	0.001
Ni	0.014	0.015	0.007	0.011	0.011	0.008
Total	3.003	2.994	3.007	3.005	3.004	2.997
Fo	94.6	95.3	93.0	95.2	94.2	92.9

CONCLUSIONS

The chromian spinel of Cheshmeh-Bid chromitites displays different major, trace and minor element compositions from that of non-equilibrated massive to disseminated chromitites. Chromian spinel in massive chromitites has retained its magmatic composition. In rare cases, alteration of chromite as high-Cr, high-Fe^{3+}, low Al_2O_3 porous spinel occurs, which is attributed to reaction between chromite and olivine in the presence of reducing fluids. However, the alteration is restricted to chromite grain boundaries and within fractures of individual chromite grains. The calculated TiO_2, Al_2O_3 and FeO/MgO contents of the parental melts of the Cheshmeh-Bid massive chromitites also indicate that these high-Cr# chromitites were derived from boninitic melts in a supra-subduction zone setting. The calculated oxygen fugacities (fO_2) or log fO_2 are +1.01, +1.43 and +0.96 in disseminated chromitites, massive chromitites and dunites, respectively. The high oxygen fugacity of the studied upper mantle from the Cheshmeh-Bid ophiolitic massif suggests a boninitic source in the mantle wedge of a suprasubduction zone. From the standpoint of trace elements, chromian spinels from the non-equilibrated massive chromitites make them analogous to chromite in typical boninites worldwide. It is crucial to note that boninitic magmatism, as inferred from chromian spinel composition, occurred all along the present-day MZT during Late Cretaceous, from the Penjween-Walash ophiolites of the northwestern Zagros Suture Zone in Kurdistan of Iraq (Aswad et al., 2011) through the Sarve-Abad ophiolites in northwestern Iran (Allahyari et al., 2014) to the study area and, possibly, to the Gogher-Baft ophiolites of southeastern Iran (Shafaii Moghadam et al., 2013). Thus, the present work confirms the widespread boninitic magmatism, extending it further to the southwest.

Table 6 - Calculated oxygen fugacities of podiform chromitites and dunite sample from the Cheshmeh-Bid chromitite deposit.

Rock type	Sample No.	Chromian spinel			Olivine		
		Mg#	Cr#	$Fe^{3+}/\Sigma Fe$	Fo (Forsterite) %	Log (fO2)	+FMQ
Massive chromitite	IRNCH210	0.63	0.79	0.21	94.63	-6.19	1.59
	IRNCH93	0.65	0.75	0.18	95.25	-6.39	1.39
Disseminated chromitite	IRNCH39	0.64	0.8	0.18	92.96	-7.27	0.51
	IRNCH201	0.69	0.67	0.21	95.18	-6.35	1.43
	IRNCH202	0.62	0.67	0.16	94.22	-6.69	1.09
Dunite	IRNCH19	0.58	0.78	0.18	92.93	-6.82	0.96

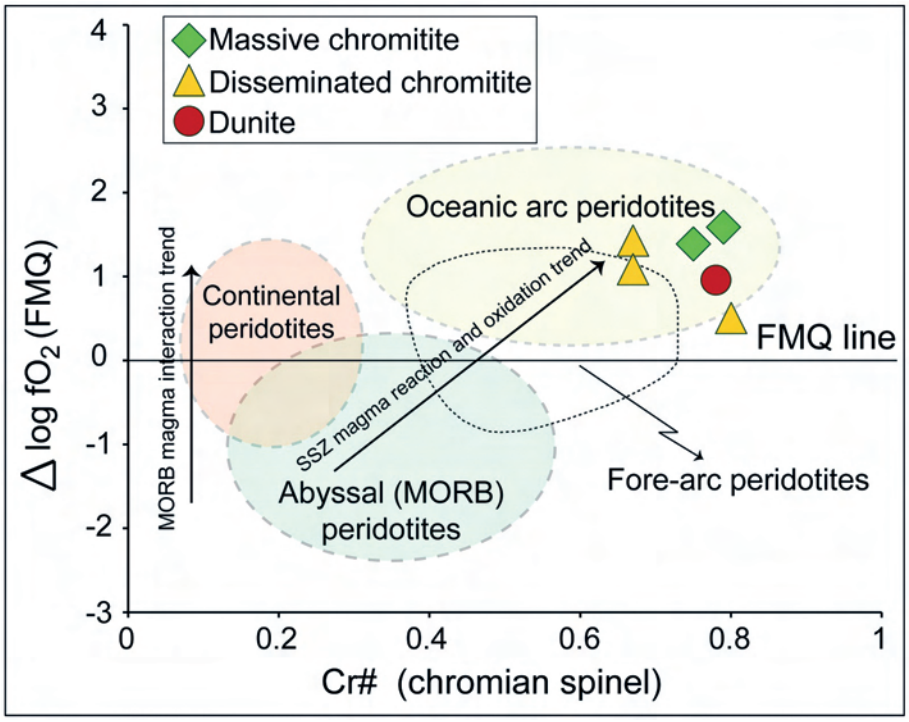

Fig. 12 - Oxygen fugacity versus Cr# of chromian spinels for the studied chromitites and associated dunite of the Cheshmeh-Bid chromitite deposit. Fields of abyssal (MORB) peridotites, oceanic-arc peridotites, fore-arc peridotites and continental peridotites are derived from Parkinson and Pearce (1998). SSZ- Supra-Subduction Zone.

ACKNOWLEDGEMENTS

The present study constitutes a part of first author's MSc thesis at Tarbiat Modares University, Tehran, Iran. The authors are grateful to Tarbiat Modares University Research Grant Council for supporting the project. Laboratory facilities at the University of Milan (Italy) and the Geochemical Analysis Unit of GEMOC, Macquarie University (Australia) are kindly appreciated for performing major and trace element analyses. We would also like to thank Emilio Saccani and Alessio Sanfilippo for their constructive reviews that helped to improve the manuscript.

REFERENCES

Alavi M., 1991. Sedimentary and structural characteristics of the Paleo-Tethys remnants in northeastern Iran. Geol. Soc. Am. Bull., 103: 983-992.

Aldanmaz E., 2012. Trace element geochemistry of primary mantle minerals in spinel peridotites from polygenetic MOR-SSZ suites of SW Turkey: constraints from an LA-ICP-MS study and implications for mantle metasomatism. Geol. J., 47 (1): 59-76.

Allahyari K., Saccani E., Pourmoafi M., Beccaluva L. and Masoudi F., 2010. Petrology of mantle peridotites and intrusive mafic rocks from the Kermanshah ophiolitic complex (Zagros belt, Iran): implications for the geodynamic evolution of the Neo-Tethyan oceanic branch between Arabia and Iran. Ofioliti, 35: 71-90.

Allahyari K., Saccani E., Rahimzadeh B. and Zeda O., 2014. Mineral chemistry and petrology of highly magnesian ultramafic cumulates from the Sarve-Abad (Sawlava) ophiolites (northwestern Iran): New evidence for boninitic magmatism in intra-oceanic fore-arc setting in the Neo-Tethys between Arabia and Iran. J. Asian Earth Sci., 79: 312-328.

Arai S., 1997. Control of wall-rock composition on the formation of podiform chromitites as a result of magma/peridotite interaction. Resour. Geol., 47: 177-187.

Arai S. and Abe N., 1994. Podiform chromitite in the arc mantle: Chromitite xenoliths from the Takashima alkali basalt, southwest Japan arc. Mineral. Dep., 19: 434-438.

Arai S. and Abe N., 1995. Reaction of orthopyroxene in peridotite xenoliths with alkali basalt melt and its implications for genesis of Alpine-type chromitite. Am. Mineral., 80: 1041-1047.

Arai S., and Matsukage K., 1998. Petrology of a chromitite micropod from Hess Deep, equatorial Pacific - a comparison between abyssal and Alpine type podiform chromitites. Lithos, 43: 1-14.

Arai S. and Yurimoto H., 1994. Podiform chromitites of the Tari-Misaka ultramafic complex, Southwest Japan, as mantle-melt interaction products. Econ. Geol., 89: 1279-1288.

Arai S., Kadoshima K. and Morishita T., 2006a. Widespread arc-related melting in the mantle section of the northern Oman ophiolite as inferred from detrital chromian spinels. J. Geol. Soc. London, 163 (5): 869-879.

Arai S., Shimizu Y., Ismail S.A. and Ahmed A.H., 2006b. Low-T formation of high-Cr spinel with apparently primary chemical characteristics within podiform chromitite from Rayat, northeastern Iraq. Mineral. Mag., 70 (5): 499-508.

Arai S., Uesugi J. and Ahmed A.H., 2004. Upper crustal podiform chromitite from the northern Oman ophiolite as the stratigraphically shallowest chromitite in ophiolite and its implication for Cr concentration. Contrib. Mineral. Petrol., 147: 145-154.

Aswad K.J.A., Aziz N.R.H. and Koy H.A., 2011. Cr-spinel compositions in serpentinites and their implications for the petrotectonic history of the Zagros Suture Zone, Kurdistan Region, Iraq. Geol. Mag., 148: 802-818.

Ballhaus C., 1998. Origin of podiform chromite deposits by magma mingling. Earth Planet. Sci. Lett., 156: 185-193.

Ballhaus C., Berry R.F. and Green D.H., 1990. Oxygen fugacity controls in the Earth's upper mantle. Nature, 348: 437-440.

Ballhaus C., Berry R.F. and Green D.H., 1991a. High pressure experimental calibration of the olivine orthopyroxene-spinel oxygen geobarometer: implications for the oxidation state of the upper mantle. Contrib. Mineral. Petrol., 107: 27-40.

Ballhaus C. Berry R.F. and Green. D.H., 1991b. Errata: High pressure experimental calibration of the olivine orthopyroxene-spinel oxygen geobarometer: implications for the oxidation state of the upper mantle: Contrib. Mineral. Petrol., 108: 384.

Barnes S.J. and Roeder P.L., 2001. The range of spinel compositions in terrestrial mafic and ultramafic rocks. J. Petrol., 42: 2279-2302.

Beccaluva L. Coltorti M. Ferrini V. Saccani E. Siena F. and Zeda O., 1998. Petrological modelling of Albanian ophiolites with particular regard to the Bulqiza chromite ore deposits. Period. Mineral., 67 (1-3): 7-23.

Bédard J.H., 1999. Petrogenesis of boninites from the Betts Cove Ophiolite, Newfoundland, Canada: Identification of subducted source components. J. Petrol., 40: 1853-1889.

Bédard J.H. and Hébert R., 1998. Formation of chromitites by assimilation of crustal pyroxenites and gabbros into peridotitic intrusions: North Arm Mountain massif, Bay of Islands ophiolite, Newfoundland, Canada. J. Geophys. Res., 103: 5165-5184.

Borisova A., Ceuleneer G., Kamenetsky V.S., Arai S., Bejina F., Abily B., Bindeman I.N., Polvé M., Parseval P., Aigouy T. and Pokrovsk G., 2012. A new view on the petrogenesis of the Oman ophiolite chromitites from microanalysis of chromite-hosted inclusions. J. Petrol., 33: 2411-2440.

Colás V., González-Jiménez J.M., Griffin W.L., Fanlo I., Gervilla F., O'Reilly S.Y., Pearson N.J., Kerestedjian T. and Proenza J.A., 2014. Fingerprints of metamorphism in chromite: New insights from minor and trace elements. Chem. Geol., 389: 137-152.

Dare S.A.S., Pearce J.A., McDonald I. and Styles M.T., 2009. Tectonic discrimination of peridotites using fO_2-Cr# and Ga-Ti-Fe^{III} systematics in chrome-spinel. Chem. Geol., 261 (3-4): 199-216.

Dick H.J.B., 1977. Partial melting in the Josephine peridotite. I. The effect on the mineral composition and its consequence for geobarometry and geothermometry. Am. J. Sci., 277: 801-832.

Dick H.J.B. and Bullen T., 1984.Chromian spinel as a petrogenetic indicator in abyssal and Alpine-type peridotites and spatially associated lavas. Contrib. Mineral. Petrol., 86: 54-76.

Dickey J.S., 1975. A hypothesis of origin for podiform chromite deposits. Geochim. Cosmochim. Acta, 39: 1061-1074.

Dilek Y., Furnes H. and Shallo M., 2008. Geochemistry of the Jurassic Mirdita Ophiolite (Albania) and the MORB to SSZ evolution of a marginal basin oceanic crust. Lithos, 100: 174-209.

Edwards S.J., Pearce J.A. and Freeman J., 2000. New insights concerning the influence of water during the formation of podiform chromitite. In: Y. Dilek, E.M. Moores, D. Elthon and A. Nicolas (Eds.), Ophiolites and oceanic crust: New insights from field studies and the Ocean Drilling Program: Boulder, Colorado, Geol. Soc. Am. Spec. Pap., 349: 139-147.

Falloon T.J. and Crawford A.J., 1991. The petrogenesis of high-calcium boninite lavas dredged from the northern Tonga ridge. Earth Planet. Sci. Lett., 102: 375-394.

Fotoohi Rad G.R., Droop G.T.R., Amini S. and Moazzen M., 2005. Eclogites and blue schists of the Sistan Suture Zone, eastern Iran: A comparison of P-T histories from a subduction mélange. Lithos, 84: 1-24.

Gervilla F., Gutiérrez-Narbona R. and Fenoll Hach-Ali P., 2002. The origin of different types of magmatic mineralizations from small-volume melts in the lherzolite massifs of the Serrania de Ronda. Bol. Soc. Españ. Mineral., 25: 79-96.

Gervilla F., Padrón-Navarta J.A., Kerestedjian T., Sergeeva I., González-Jiménez J.M. and Fanlo I., 2012. Formation of ferrian chromite in podiform chromitites from the Golyamo Kamenyane serpentinite, Eastern Rhodopes, SE Bulgaria: a two-stage process. Contrib. Mineral. Petrol., 164: 643-657.

Gervilla F., Proenza J.A., Frei R., González-Jiménez J.M., Garrido C.J., Melgarejo J.C., Meibom A., Díaz-martínez R. and Lavaut W., 2005. Distribution of platinum-group elements and Os isotopes in chromite ores from Mayarí-Baracoa Ophiolilte Belt (eastern Cuba). Contrib. Mineral. Petrol., 150: 589-607.

Ghazi A.M. and Hassanipak A.A., 1999. Geochemistry of subalkaline and alkaline extrusives from the Kermanshah ophiolite, Zagros Suture Zone, western Iran: implications on Tethyan plate tectonics. J. Asian Earth Sci., 17: 319-332.

Ghazi A.M., Hassanipak A.A., Mahoney J.J. and Duncan R.A., 2004. Geochemical characteristics, ^{40}Ar-^{39}Ar ages and original tectonic setting of the Band-e-Zeyarat/Dar Anar ophiolite, Makran accretionary prism, S.E. Iran. Tectonophysics, 393: 175-196.

González-Jiménez J.M., Augé T., Gervilla F., Bailly L., Proenza J.A. and Griffin W.L., 2011. Mineralogy and geochemistry of platinum-rich chromitites from the mantle-crust transition zone at Ouen Island, New Caledonia Ophiolite. Can. Mineral., 49 (6): 1549-1569.

González-Jiménez J.M., Griffin W.L., Gervilla F., Proenza J.A., O'Reilly S.Y. and Pearson N.J., 2014. Chromitites in ophiolites: how, where, when, why? Part II. The crystallization of chromitites. Lithos, 189: 140-158.

González-Jiménez J.M., Locmelis M., Belousova E., Griffin W.L., Gervilla F., Kerestedjian T.N., Pearson N.J. and Sergeeva I., 2015. Genesis and tectonic implications of podiform chromitites in the metamorphosed Ultramafic Massif of Dobromirtsi (Bulgaria). Gondwana Res., 27: 555-574.

Greenbaum D., 1977. The chromitiferous rocks of the Troodos ophiolite complex, Cyprus. Econ. Geol., 72: 1175-1195.

Grieco G., Ferrario A. and Mathez E.A., 2004. The effect of metasomatism on the Cr-PGE mineralization in the Finero Complex, Ivrea Zone, Southern Alps. Ore Geol. Rev., 24: 299-314.

Griffin W.L., Powell W.J., Pearson N.J. and O'Reilly S.Y., 2008. GLITTER: data reduction software for laser ablation ICP-MS (appendix). In: P. Sylvester (Ed.), Laser Ablation-ICP-MS in the Earth Sciences. Mineral. Ass. Can., Short Course Ser., 40: 204-207.

Hichey R. and Frey F.A., 1982. Geochemical characteristics of boninite series volcanics: Implications for their sources. Geochim. Cosmochim. Acta, 46: 2099-2115.

Kamenetsky V.S., Crawford A.J. and Meffre S., 2001. Factors controlling chemistry of magmatic spinel: An empirical study of associated olivine, Cr-spinel and melt inclusions from primitive rocks. J. Petrol., 42: 655-671.

Lago B., Rabinowicz M. and Nicolas A., 1982. Podiform chromite ore bodies: a genetic model. J. Petrol., 23: 103-125.

Leblanc M. and Ceuleneer G., 1992. Chromite crystallization in a multicellular magma flow: evidence from a chromitite dike in the Oman ophiolite. Lithos, 27: 231-257.

Leblanc M. and Nicolas A., 1992. Ophiolitic chromitites. Int. Geol. Rev. 34: 653-686.

Maurel C. and Maurel P., 1982. Étude expérimentale de la distribution de l'aluminium entre bain silicaté basique et spinelle chromifère. Implications pétrogénétiques: teneur en chrome des spinelles. Bull. Minéral., 105: 197-202.

McCall G.J.H., 1985. Explanatory text of the Minab Quadrangle Map 1:250000 J13. Geol. Surv. Iran.

McCall G.J.H., 1997. The geotectonic history of the Makran and adjacent areas of southern Iran. J. Asian Earth Sci., 15: 517-531.

McElduff B. and Stumpfl E.F., 1991. The chromite deposits of the Troodos Complex, Cyprus- evidence for the role of a fluid phase accompanying chromite formation. Miner. Dep., 26: 307-318.

Melcher F., Grum W., Simon G., Thalhammer T.V. and Stumpfl E.F., 1997. Petrogenesis of the ophiolitic giant chromite deposits of Kempirsai, Kazakhstan: a study of solid and fluid inclusions in chromite. J. Petrol., 38: 1419-1458.

Merlini A., Grieco G., Ottolini L. and Diella V., 2011. Probe and SIMS investigation of clinopyroxene inclusions in chromite from the Troodos chromitites (Cyprus): implications for dunite-chromitite genesis. Ore Geol. Rev., 41: 22-34.

Nadimi A., 2002. Mantle flow patterns at the Neyriz Paleo-spreading center, Iran. Earth Planet. Sci. Lett., 203: 93-104.

Omrani H., Moazzen M., Oberhansli R., Altenberger U. and Lange M., 2013. The Sabzevar blue schists of the North-Central Iranian micro-continent as remnants of the Neotethys-related oceanic crust subduction. Int. J. Earth Sci., 102: 1491-1512.

Pagé P. and Barnes S.J., 2009. Using trace elements in chromites to constrain the origin of podiform chromitites in the Thetford Mines ophiolite, Québec, Canada. Econ. Geol., 104 (7): 997-1018.

Paktunc A.D., 1990. Origin of podiform chromite deposits by multistage melting, melt segregation and magma mixing in the upper mantle. Ore Geol. Rev., 5: 211-222.

Paktunc A.D. and Cabri L.J., 1995. A proton- and electron-microprobe study of gallium, nickel and zinc distribution in chromian spinel. Lithos, 35: 261-282.

Parkinson I.J. and Arculus R.J., 1999. The redox state of subduction zones: insights from arc-peridotites. Chem. Geol., 160: 409-423.

Parkinson I.J. and Pearce J.A., 1998. Peridotites of the Izu-Bonin-Mariana forearc (ODP Leg 125) evidence for mantle melting and melt-mantle interactions in a suprasubduction zone setting. J. Petrol., 39: 1577-1618.

Pearce J.A., Barker P.F., Edwards S.J., Parkinson I.J. and Leat, P.T., 2000. Geochemistry and tectonic significance of peridotites from the South Sandwich arc-basin system, South Atlantic. Contrib. Mineral. Petrol., 139 (1): 36-53.

Proenza J.A., Gervilla F., Melgarejo J.C. and Bodinier J.L., 1999. Al- and Cr-rich chromitites from the Mayarí-Baracoa Ophiolitic Belt (Eastern Cuba): consequence of interaction between volatile-rich melts and peridotites in suprasubduction mantle. Econ. Geol., 94: 547-566.

Rajabzadeh M.A., 1998. Mineralisation en chromite et elements du groupe du platine dans les ophiolites d'Assemion et de Neyriz, ceinture du Zagros, Iran. Ph. D. Thesis, Inst. Nation. Polytechn. Lorraine, France, 358 pp.

Rajabzadeh M.A. and Moosavinasab Z., 2012. Mineralogy and distribution of platinum-group minerals (PGM) and other solid inclusions in the Neyriz ophiolitic chromitite, southern Iran. Can. Mineral., 50: 643-665.

Rajabzadeh M.A. and Nazari-Dehkordi T., 2013. Investigation on mantle peridotites from Neyriz ophiolite, south of Iran: geodynamic signals. Arab. J. Geosci., 6: 4445-4461.

Rajabzadeh M.A., Nazari-Dehkordi T. and Caran S., 2013. Mineralogy, geochemistry and geotectonic significance of mantle peridotites with high-Cr chromitites in the Neyriz ophiolite from the outer Zagros ophiolite belts, Iran. J. Afr. Earth. Sci., 78: 1-15.

Roeder P.L. and Reynolds I., 1991. Crystallization of chromite and chromium solubility in basaltic melts. J. Petrol., 32: 909-934.

Rollinson H., 2008. The geochemistry of mantle chromitites from the northern part of the Oman ophiolite: inferred parental melt compositions. Contrib. Mineral. Petrol., 156: 273-288.

Saccani E. and Tassinari R., 2015. The role of morb and SSZ magma-types in the formation of Jurassic ultramafic cumulates in the Mirdita ophiolites (Albania) as deduced from chromian spinel and olivine chemistry. Ofioliti, 40: 37-56.

Saccani E., Allahyari K., Beccaluva L. and Bianchini G., 2013b. Geochemistry and petrology of the Kermanshah ophiolites (Iran): implication for the interaction between passive rifting, oceanic accretion, and plume-components in the Southern Neo-Tethys Ocean. Gondwana Res., 24: 392-411.

Saccani E., Allahyari K. and Rahimzadeh B., 2014. Petrology and geochemistry of mafic magmatic rocks from the Sarve-Abad ophiolites (Kurdistan region, Iran): Evidence for interaction between MORB-type asthenosphere and OIB-type components in the southern Neo-Tethys Ocean. Tectonophysics, 621: 132-147.

Saccani E., Azimzadeh Z., Dilek Y. and Jahangiri A., 2013a. Geochronology and petrology of the Early Carboniferous Misho Mafic Complex (NW Iran), and implications for the melt evolution of Paleo-Tethyan rifting in Western Cimmeria. Lithos, 162-163: 264-278.

Saccani E., Beccaluva L., Photiades A. and Zeda O., 2011. Petrogenesis and tectonomagmatic significance of basalts and mantle peridotites from the Albanian-Greek ophiolites and sub-ophiolitic mélanges. New constraints for the Triassic-Jurassic evolution of the Neo-Tethys in the Dinaride sector. Lithos 124: 227-242.

Saccani E., Delavari M., Beccaluva L. and Amini S.A., 2010. Petrological and geochemical constraints on the origin of the Nehbandan ophiolitic complex (eastern Iran): implication for the evolution of the Sistan Ocean. Lithos, 117: 209-228.

Saccani E., Photiades A., Santato A. and Zeda O., 2008. New evidence for suprasubduction zone ophiolites in the Vardar zone from the Vermion massif (northern Greece): implication for the tectono-magmatic evolution of the Vardar oceanic basin. Ofioliti, 33: 65-85.

Sack R.O. and Ghiorso M.S., 1991. Chromian spinels as petrogenetic indicators: Thermodynamics and petrological applications. Am. Mineral., 76: 827-847.

Shafaii Moghadam H., and Stern R.J., 2011. Geodynamic evolution of Upper Cretaceous Zagros ophiolites: Formation of oceanic lithosphere above a nascent subduction zone. Geol. Mag., 148: 762-801.

Shafaii Moghadam H.S., Stern R.J., Chiaradia M. and Rahgoshay M., 2013. Geochemistry and tectonic evolution of the Late Cretaceous Gogher-Baft ophiolite, central Iran. Lithos, 168-169: 33-47.

Shi R., Griffin W.L., O'Reilly S., Huang Q., Zhang X., Liu D., Zhi X., Xia Q. and Ding L., 2012. Melt/mantle mixing produces podiform chromite deposits in ophiolites: implications of Re-Os systematics in the Dongqiao Neo-Tethyan ophiolite, northern Tibet. Gondwana Res., 21: 194-206.

Shojaat B., Hassanipak A.A., Mobasher K. and Ghazi A.M., 2003. Petrology, geochemistry and tectonics of the Sabzevar ophiolite, North Central Iran. J. Asian Earth Sci., 21: 1053-1067.

Stöcklin J., 1974. Possible ancient continental margins in Iran. In: C.A. Burke and C.L. Drake (Eds.), The geology of continental margins. Springer, NewYork, p. 873-887.

Takin M., 1972. Iranian geology and continental drift in the Middle East. Nature, 235: 147-150.

Taylor R.N., Nesbitt R.W., Vidal P., Harmon R.S., Auvray B. and Croudace I.W., 1994. Mineralogy, chemistry, and genesis of the boninite series volcanics, Chichijima, Bonin Islands, Japan. J. Petrol., 35: 577-617.

Tirrul R., Bell I.R., Griffis R.J. and Camp V.E., 1983. The Sistan suture zone of eastern Iran. Geol. Soc. Am. Bull., 94: 134-150.

Zarrinkoub M.H., Pang K-N., Chung S-L., Khatib M.M., Mohammadi S.S., Chiu H-Y. and Lee H-Y., 2012. Zircon U-Pb age and geochemical constraints on the origin of the Birjand ophiolite, Sistan suture zone, eastern Iran. Lithos, 154: 392-405.

Zhou M.F., Keays R.R. and Kerrich R.W., 1998. Controls on platinum-group elemental distributions of podiform chromitites: a case study of high-Cr and high-Al chromitites from Chinese orogenic belt. Geochim. Cosmochim. Acta, 62: 677-688.

Zhou M.F., Robinson P.T. and Bai W.J., 1994. Formation of podiform chromites by melt-rock interaction in the upper mantle. Miner. Dep., 29: 98-101.

Zhou M.F., Robinson P.T., Malpas J., Aitchison J., Sun M., Bai W.J., Hu X.F. and Yang J.-S., 2001. Melt/mantle interaction and melt evolution in the Sartohay high-Al chromite deposits of the Dalabute ophiolite (NW China). J. Asian Earth. Sci., 19: 517-534.

Zhou M.F., Robinson P.T., Malpas J. and Zijin L., 1996. Podiform chromites in the Luobusa Ophiolite (Southern Tibet): implications for melt–rock interaction and chromite segregation in the upper mantle. J. Petrol., 37: 3-21.

Received, June 26, 2015
Accepted, October 27, 2015